

# Feedback Upon Dust Emission By Dust Radiative Forcing Through the Planetary Boundary Layer

R. L. Miller,<sup>1,2</sup> J. Perlwitz,<sup>1,2</sup> and I. Tegen<sup>3</sup>

## Abstract.

Large changes to the amount of airborne soil particles (or ‘mineral dust’ aerosol) inferred from the climate record raise the question of whether radiative forcing by dust particles amplifies or else diminishes these changes. A previous study with an atmospheric general circulation model (AGCM) indicates that dust radiative forcing in the present-day climate reduces emission of dust into the atmosphere. Here, we interpret this reduction as an interaction between dust radiative forcing and the planetary boundary layer (PBL). By reducing sunlight incident upon the surface, dust decreases the turbulent flux of sensible heat into the atmosphere. This reduces turbulent mixing within the PBL, along with the downward transport of momentum to the surface, resulting in a decrease of surface wind speed and dust emission. We illustrate this mechanism by comparing the diurnal cycle of emission simulated by two versions of an AGCM, one containing dust radiative forcing, and the other with this forcing set to zero. At some of the most productive source regions, morning emission is reduced in proportion to the surface radiative forcing. We suggest that this negative feedback may be underestimated by the AGCM.

## 1. Introduction

Airborne soil particles (or ‘mineral dust’ aerosol) alter the atmospheric circulation by scattering sunlight and changing the radiative budget of the earth [Miller and Tegen, 1998]. These circulation changes feed back upon the wind erosion of particles at the surface and the aerosol load overhead [Perlwitz *et al.*, 2001]. The expansion of Martian dust storms from regional to global scale is hypothesized to occur through a feedback upon wind erosion by dust radiative forcing and associated changes to the circulation [Kahn *et al.*, 1992; Read and Lewis, 2004]. Large changes in the terrestrial dust load are inferred from the paleoclimatic record. At the transition from the Paleocene to the Eocene, roughly 55 million years ago, dust deposition dropped substantially downwind of Asian source regions, and has since remained low [Rea, 1994]. During glacial times, dust deposition over high latitude ice sheets increased by an order of magnitude compared to the present value [Biscaye *et al.*, 1997]. Within the twentieth century, rainfall records suggest that production of Sahel dust varied by a factor of two [Prospero and Lamb, 2003]. These examples raise the question of whether changes in dust radiative forcing amplify or else diminish the perturbation to the dust load by the changing climate.

Perlwitz *et al.* [2001] calculate that within the current climate, the effect of dust radiative forcing is to reduce the global dust load. In this article, we consider mechanisms by which this reduction takes place. Dust

---

<sup>1</sup>Department of Applied Physics and Applied Math,  
Columbia University, New York, New York, USA.

<sup>2</sup>NASA Goddard Institute for Space Studies, New York,  
New York, USA.

<sup>3</sup>Max Planck Institute for Biogeochemistry, Jena,  
Germany.

radiative heating reduces the strength of the tropical circulation by offsetting the clear-sky longwave cooling by greenhouse gases that is otherwise balanced by adiabatic subsidence [Miller and Tegen, 1999]. A reduction in tropical overturning diminishes the surface winds that lift dust particles into the atmosphere. However, *Perlwitz et al.* [2001] show that for the current climate, only in a few locations is the reduction in the intensity of the quasi-steady tropical circulation by dust correlated with a reduction in dust emission. Changes to this circulation by the present-day dust load are apparently too small to affect emission. Observations and laboratory measurements demonstrate that emission is a highly non-linear function of wind speed, and that intense albeit infrequent gusts contribute a disproportionate amount to the total emission [Shao, 2000]. *Perlwitz et al.* [2001] suggest that the feedback between dust radiative forcing and emission is dominated by time scales that are short compared to the slow seasonal variations of the tropical circulation.

Wind erosion of dust is related to the surface wind stress, which is controlled by the downward transport of momentum within the planetary boundary layer (PBL). Mixing within the PBL is driven in part by the buoyancy flux at the surface in response to solar heating [Arya, 1988]. As the sun passes overhead, the surface wind increases as momentum from stronger winds aloft is mixed downward. *N'Tchayi Mbourou et al.* [1997] show that dust emission within the Sahel has a strong diurnal cycle, related to the daily development of the planetary boundary layer (PBL). Over the Sahara, dust is mixed to great heights by the diurnal expansion of the PBL [Carlson and Prospero, 1972]. In arid regions that favor dust emission, the buoyancy flux is dominated by the surface flux of sensible heat, which is tightly coupled to solar heating. By reducing the sunlight incident upon the surface, dust has the potential to decrease the vigor of PBL mixing and the surface wind that controls emission.

In this article, we examine how dust radiative forcing interacts with the planetary boundary layer to feed back upon emission. We calculate this interaction using a model of the dust aerosol life cycle embedded within an Atmospheric General Circulation Model (AGCM), described in Section 2. In Section 3, we identify the time scales dominating emission and its reduction by dust radiative forcing. We find that for the regions producing the most dust, there are substantial diurnal variations in emission, associated with the daily development of the PBL. In section 4, we describe the interaction of dust radiative forcing with the PBL, and propose that this is an important mechanism by which emission is reduced in the study of *Perlwitz et al.* [2001]. We assess whether our model's representation of the feedback between dust radiative forcing and emission is realistic, and likely to operate in other dust aerosol models. Our conclusions are presented in Section 5, where we summarize the physical processes that must be included within a model in order to represent this feedback.

## 2. Model Description

The calculation of the dust distribution within the NASA Goddard Institute for Space Studies (GISS) AGCM is based upon the offline aerosol model developed by *Tegen and Fung* [1994]. The size and spatial distribution of dust is calculated as a function of the model climate [Tegen and Miller, 1998]. By scattering and absorbing radiation, dust particles feed back upon the climate and thus upon their own distribution [Perlwitz et al., 2001]. In the experiments described below, the

model climatology and dust radiative forcing are nearly identical to values reported by *Miller et al.* [2004b]. Here, we summarize aspects of the model that are relevant to the interaction of dust with the PBL, referring the reader to the above articles for a more complete description.

This version of the NASA GISS AGCM has horizontal resolution of  $4^\circ$  latitude by  $5^\circ$  longitude, with 12 layers extending from the surface to 10 mb [*Hansen et al.*, 2002]. Tracers, including dust, are advected using a quadratic upstream scheme that accounts for the value of the tracer at each grid box, along with its slope and curvature [*Prather*, 1986], resulting in tracer resolution on a finer scale than the nominal grid box dimensions. Dust emission is a function of the surface wind, as described below, which depends upon turbulent transport of momentum to the surface. Turbulent transport is calculated on a separate 8-level grid extending from the middle of the lowest AGCM layer to the surface, a depth of roughly 200 m that defines the model PBL. Based upon a second-order closure scheme [*Mellor and Yamada*, 1982; *Galperin et al.*, 1988], transport is derived by assuming a local balance between the dissipation of turbulent kinetic energy and its generation by shear and buoyancy [*Hartke and Rind*, 1997].<sup>1</sup> Mixing by subgrid circulations above the first AGCM layer is accomplished by parameterizations of dry and moist convection.

Emission occurs in the model when the winds are sufficiently strong in regions where abundant soil particles are loosely bound to the surface as a result of low soil moisture. Regions containing erodible particles are identified using the desert, grass, and shrub categories within the vegetation data set of *Matthews* [1983]. This allows dust emission to occur potentially over a third of the land surface [*Tegen and Fung*, 1994]. Recent studies have identified the dry beds of former lakes as sites of enhanced emission [*Gimoux et al.*, 2001; *Tegen et al.*, 2002; *Zender et al.*, 2003a], and incorporation of these features results in more precise agreement with satellite retrievals of aerosol optical thickness in the vicinity of dust sources [*Zender et al.*, 2003b]. While our omission of preferred sources possibly distorts the geographic distribution of the AGCM feedback between dust radiative forcing and emission, we assume the identity of the physical processes comprising the feedback is not sensitive to this omission.

Based upon wind tunnel measurements, emission occurs when the shear stress at the surface exceeds a threshold value [*Shao*, 2000]. The shear stress is related to the surface wind speed according to the stability of the surface layer and roughness of the surface. We assume a uniform value of surface roughness for all source regions, and recast the formula for emission  $\mathcal{E}$  in terms of surface wind speed  $u_s$ :

$$\mathcal{E} = C u_s^2 (u_s - u_T) \text{ for } u_s \geq u_T, \quad (1)$$

where  $C$  is an empirically derived coefficient of proportionality, and  $u_T$  is a threshold, below which emission is zero. Experiments indicate that observed wind speeds are too low to directly erode particles with radii smaller than  $10 \mu\text{m}$  that dominate the global dust burden and radiative forcing [*Shao et al.*, 1993]. Instead, these particles are liberated by the impact of larger particles whose radii are of order  $30 \mu\text{m}$  and larger [*Alfaro and Gomes*, 2001], and which are less tightly bound to the surface by cohesive forces. Our threshold for emission represents the minimum wind speed required to mobilize these larger particles.

The surface wind speeds computed by the AGCM are generally smaller than the high-resolution European Cen-

ter for Medium-Range Weather Forecast reanalysis values used to calculate emission in an offline transport model [Tegen and Miller, 1998]. Because of its lower resolution, the AGCM fails to reproduce the highest values of surface wind speed present in the reanalyses that account for the most emission. To account for wind fluctuations on scales too small to be represented by the AGCM, Tegen and Miller [1998] adjusted the threshold  $u_T$  at each grid box so that the AGCM surface concentration compared well to observed values. (The value of this threshold relative to the surface wind speed determines emission according to Eq. 1.) Subsequent improvements to the AGCM parameterization of the PBL have altered the surface winds, so that this comparison has been slightly degraded. Nonetheless, the model continues to reproduce the general features of the observed seasonal evolution of the dust distribution [Perlwitz et al., 2001]. Subgrid fluctuations in wind speed have been subsequently parameterized by Cakmur et al. [2004], although this effect is not included in this model. Below we suggest that the prescribed geographic variations of the threshold distort the feedback of dust radiative forcing upon emission, although this does not change the fundamental mechanism we describe.

Dust particles are transported according to particle size within four categories. For the radiation calculation, the three silt categories are assigned effective radii of 1, 2, and 4  $\mu\text{m}$ . Clay particles, although transported as a single category, are further divided into 4 subcategories with effective radii of 0.1, 0.2, 0.4 and 0.8  $\mu\text{m}$ , using the mass partitioning computed explicitly by Tegen and Lacis [1996]. Scattering is modeled using Mie theory [van de Hulst, 1957], and in addition to particle size, depends upon the dust index of refraction. This index is taken from laboratory measurements at solar [Patterson et al., 1977] and thermal wavelengths [Volz, 1973] using far-traveled Saharan dust collected over the Atlantic. Scattering in the longwave is neglected compared to absorption. Dufresne et al. [2002] show that this results in an underestimate of longwave forcing, although Miller et al. [2004b] calculate that this is a small omission to the total forcing, especially at the surface. Calculation of dust radiative forcing is described in greater detail by Tegen and Lacis [1996], along with Lacis and Mishchenko [1995].

To compute the feedback upon emission by dust radiative forcing, we compare the dust cycle between two experiments. One contains dust radiative forcing, while the second (or control) omits this forcing, despite its inclusion of dust. Differences between the experiments represent the feedback of forcing upon the dust cycle. To allow the ocean surface to respond to dust radiative forcing, sea surface temperature (SST) is calculated using a mixed-layer model [Miller et al., 1983]. SST varies according to the net surface heat flux calculated by the AGCM, along with a prescribed seasonal cycle of ocean heat transport. (The latter is prescribed to balance the net surface heat flux in an integration with specified SST.) The first 19 years of each experiment, when the ocean mixed layer comes into equilibrium with dust radiative forcing, are discarded. The subsequent 31 years are used to compute the climatology of each experiment.

Recent in situ measurements of absorption by dust particles at solar wavelengths suggest that our adopted indices of refraction are excessively absorbing [Kaufman et al., 2001; Dubovik et al., 2002; Sinyuk et al., 2003]. Moreover, these indices vary regionally according to the mineral composition of the source [Sokolik et al., 1993], contrary to our use of a globally uniform value. To calcu-

late the sensitivity of the emission feedback to these variations, we carry out two additional experiments where the particle single scatter albedo  $\varpi$  is increased or else decreased by ten percent (although never allowed to exceed unity). Total extinction is held constant so that a 10 percent decrease in  $\varpi$  corresponds to an increase in absorption at the expense of scattering. *Miller et al.* [2004b] calculate that for the ‘baseline’ experiment using Saharan optical properties (denoted by ‘ $1.0 \times \varpi$ ’), the global average of the dust single scatter albedo is 0.905 in the spectral band between 0.20 and 0.77  $\mu\text{m}$ . A 10 percent reduction in  $\varpi$  (the experiment denoted by ‘ $0.9 \times \varpi$ ’) results in a near doubling of absorption (proportional to  $1 - \varpi$  for  $\varpi$  near unity). Conversely, a 10 percent increase (the experiment denoted by ‘ $1.1 \times \varpi$ ’) corresponds to particles that are almost totally reflecting. The prescribed variation of the particle single scatter albedo gives us three experiments that can be compared to the dust cycle calculated in the absence of dust radiative forcing.

While the experiments differ only in their radiative forcing, internal variability also contributes to differences in model behavior, and may obscure the effect of forcing upon dust emission. In general, differences between the experiments that we discuss below are statistically significant around the 95% confidence level or higher, as a result of our long model integrations. For emission, which is archived by the AGCM each hour, the standard deviation used to estimate the confidence level is based upon hourly values. Other variables are available only as monthly averages, and their standard deviation is based upon interannual variations. While internal variability contributes to differences between the experiments, our statistical tests suggest that the differences we discuss below are predominately due to differences in dust radiative forcing.

### 3. Time Variation of Emission

In the absence of radiative forcing by dust particles, global annual emission is  $1162 \pm 110 \text{ Tg}$  (Figure 1a). For comparison, *Perlwitz et al.* [2001] report emission of  $1312 \text{ Tg}$ , based upon an identical model but with prescribed SST at the lower boundary. While emission is slightly lower in the present study, the climatological distribution of dust is nearly identical between the two models, with a median spatial correlation of 0.95 over the twelve months of the seasonal cycle. The model of *Perlwitz et al.* [2001] generally underestimates oceanic retrievals of dust optical thickness by the Advanced Very High Resolution Radiometer [*Husar et al.*, 1997], suggesting that the model burden is too low, even though the observed spatial distribution is successfully reproduced. Our emission is also at the lower end of values calculated by current dust models [*Miller et al.*, 2004b]. Both these suggest that the radiative forcing and feedback upon emission calculated by our model may be underestimated.

The inclusion of dust radiative forcing reduces emission by roughly 15% (Figure 1a), indicating a negative feedback. Table 1 shows the global and annual average radiative forcing, along with the fractional reduction in emission. While the magnitude of forcing at the surface increases steadily with particle absorption, the fractional reduction in global emission is largely insensitive to this increase. Although the inclusion of dust radiative forcing reduces emission in all experiments, there is no simple relation between this reduction and the forcing.

Figure 1 shows that while emission is reduced worldwide, the dependence of this reduction upon particle

absorption varies regionally. For example, the experiment with more absorbing particles ( $0.9 \times \varpi$ ) exhibits the largest reduction over East Asia and North America (Figure 1e,f), but the smallest reduction over Central Asia (Figure 1d). The reduction of emission is generally consistent with that calculated by *Perlwitz et al.* [2001], whose Table 1 can be compared with our Figure 1. The main difference resulting from our use of a mixed-layer ocean is the absence of a positive feedback between dust radiative forcing and emission over Arabia, associated with the Asian monsoon during Northern Hemisphere (NH) summer. This contrast is discussed separately [*Miller et al.*, 2004a].

Although one-third of the land area has the potential to emit dust [*Tegen and Fung*, 1994], emission is dominated by a few prolific locations. Figure 2 shows that the thirty most productive grid boxes — corresponding to roughly 3% of the land area — emit two-thirds of the global total. Eight sites in particular emit one-third of the total. *Prospero et al.* [2002] argue that loose soil particles, susceptible to wind erosion, are not ubiquitous, but are concentrated in regions like dry lake beds. Our model lacks such concentrated ‘preferred sources.’ The disproportionate emission within a few prolific grid boxes illustrates that the high winds making the greatest contribution to emission are also not ubiquitous, but are more likely in specific regions.

The reduction of emission by dust radiative forcing is in contrast to the apparent insensitivity of the reduction to the actual value of the forcing. Given a possible non-linear relation between dust emission and surface radiative forcing, we consider whether there is a more clear relationship between these quantities at shorter time scales that is obscured by our annual averaging. To identify the time scales that contribute to the variability of emission, we compute power spectra using ten years of hourly emission values from each experiment. Figure 3 shows the contribution at each frequency to the variance of emission at the four most productive grid boxes for the experiment omitting dust radiative forcing. At each location, spectra are computed over one-year intervals successively offset by six months, and then averaged together. This preserves cycles that are consistently present within each interval (like the annual and diurnal cycles), while diminishing cycles that are prominent in only a few of the intervals, and which therefore are not robust [*Welch*, 1967; *Press et al.*, 1992]. The seasonal evolution of the dust burden, as represented by the annual harmonic and its overtones, is prominent at most locations, consistent with observations of surface concentration, [*Prospero et al.*, 1981], satellite retrievals of dust optical thickness [*Husar et al.*, 1997; *Herman et al.*, 1997], and models [*Tegen and Fung*, 1994]. In addition to the annual cycle, most locations show prominent peaks at the diurnal frequency along with its higher harmonics. The diurnal cycle of emission is especially prominent over the Sahara desert (Figure 3a), where solar heating is observed to create a deep midday boundary layer [*Carlson and Prospero*, 1972]. Our estimate at the semi-diurnal frequency is large compared to the estimate by *Luo et al.* [2004], based upon a dust transport model driven by the National Center for Environmental Prediction reanalyses. In the next section, we argue that the large semi-diurnal contribution to the diurnal cycle of dust emission is the result of unrealistic behavior by the PBL parameterization.

Beside peaks representing the annual and diurnal cycles, the spectrum varies smoothly. Power increases toward lower frequencies, as typical of many geophysical spectra. Except for the annual cycle, the spectrum is

white at periods longer than a few days, and exhibits no preferred time scale. Both observations and other models indicate that surface wind fluctuations with a period of few days contribute to dust emission in the western Sahara region [Westphal *et al.*, 1988; Jones *et al.*, 2003; Luo *et al.*, 2004]. These fluctuations are the surface signature of African waves — synoptic scale disturbances that originate as shear instabilities within the low-level African Easterly Jet [Burpee, 1972]. African wave variability is underestimated by the AGCM [Druryan and Hall, 1994], which might obscure any feedback by dust radiative forcing at this time scale.

While sampling the 10 year record within overlapping one-year subsets reduces the influence of noise, this precludes spectral estimation at periods longer than one year. Spectra of the entire ten year record (not shown) do not depart significantly from the smooth spectrum at these longer superannual periods. The only distinctive time scales of dust emission in our model are the annual and diurnal cycle forced by variations in solar radiation.

The emission spectra for the experiments with dust radiative forcing are qualitatively similar to those in Figure 3, which are calculated for the experiment omitting this forcing. For comparison, the spectral estimates for the radiatively active experiments are superimposed on this figure, although for clarity only at the frequencies comprising the diurnal cycle. In general, dust radiative forcing reduces the spectral power at the diurnal harmonics, and this reduction increases with the magnitude of the surface radiative forcing by dust (Table 2). To quantify the reduction in the diurnal cycle of emission, Figure 4 shows at the four most productive dust sources the difference in spectral power between the baseline experiment with dust radiative forcing ( $1.0 \times \varpi$ ) and the experiment omitting this forcing. In addition, the spectral difference for the experiments with more absorbing ( $0.9 \times \varpi$ ) and more reflecting ( $1.1 \times \varpi$ ) particles are shown with respect to the experiment without forcing, although only at the diurnal harmonics. (Note the absence of a logarithmic scale in this figure, in comparison to Figure 3.) In Figure 4, the reduction of emission by dust radiative forcing is indicated by negative values. In some locations, like the Central Asia grid box (Figure 4c), there is no preferred time scale for the feedback. However, at certain locations, the diurnal and annual time scales that contribute predominately to emission also dominate the feedback by dust radiative forcing. In the western Sahara, the difference is almost entirely at diurnal scales, while the annual cycle is also important in the Australian desert. This suggests that in these locations, the relation between dust radiative forcing and its feedback upon emission may be apparent in the diurnal cycle.

#### 4. Dust Radiative Forcing and the Planetary Boundary Layer

In this section, we examine to what extent the reduction of boundary layer mixing by dust radiative forcing can account for the weaker surface wind and diminished emission of dust at certain locations in the AGCM.

The surface response to dust radiative forcing is given by Figure 5 for the thirty most prolific sources (identified in Figure 2). At these locations, surface forcing is regressed against annual mean anomalies of the net radiative flux into the surface, sensible heat flux into the atmosphere, wind speed, and dust emission. Anomalous values for each experiment with dust radiative forcing are defined by subtracting the corresponding value from the control experiment, where a dust cycle is calculated but

its radiative forcing is set to zero. The anomaly represents the response to dust radiative forcing. The exception is for radiative fluxes, where the anomaly consists of the forcing in addition to the response. A comparison of Figure 5a and Table 1 shows that the net radiative anomaly into the surface is nearly as large as the forcing (for the baseline experiment,  $-8.3 \text{ Wm}^{-2}$  versus  $-10.2 \text{ Wm}^{-2}$ ). Thus, the surface radiative response is small. In comparison, for an atmosphere in radiative equilibrium, the surface radiative response is equal and opposite to the forcing through a reduction in the the upward longwave flux by cooling of the surface. The small AGCM radiative response indicates that the surface forcing is balanced mainly by the turbulent fluxes of latent and sensible heat, whose relative contribution depends in a subtle way upon boundary layer dynamics and the available soil moisture [Yu *et al.*, 2002]. Globally, the forcing is compensated predominately by the surface latent heat flux [Miller and Tegen, 1998]. However, soil moisture available for evaporation is low where dust is emitted, and compensation of the surface radiative forcing is mainly through a reduction in the sensible heat flux back into the atmosphere (Figure 5b).

This compensation is consistently exhibited within the most productive emitting locations. Not only is the average of the sensible heat flux anomaly over all locations comparable to the forcing (for the baseline experiment,  $-8.3 \text{ Wm}^{-2}$  versus  $-10.2 \text{ Wm}^{-2}$ ), but the relation is highly consistent among the most productive sources. The value of  $r^2$  listed in each panel of Figure 5 indicates the fraction of variance represented by the linear regression. The fraction is typically larger in the baseline and more absorbing ( $0.9 \times \varpi$ ) experiments, where the magnitude of the forcing is largest. In the baseline experiment, the regression in Figure 5b accounts for nearly 80% of the variability of the sensible heat flux, given variations in forcing from one location to the next.

Over the dry terrain favorable to dust emission, the surface flux of sensible heat makes the predominant contribution to the surface buoyancy flux. The latter drives mixing within the boundary layer, bringing momentum from the relatively fast winds aloft to the surface. However, the relationship between forcing and surface wind speed along with emission (Figures 5c and d) is weaker than for the sensible heat flux, at least for annually averaged anomalies. Their correlation is only marginally significant in the baseline experiment (Table 3). When averaged over the most productive source regions (inset box of Figure 5d), the experiment with the more absorbing particles ( $0.9 \times \varpi$ ) exhibits the smallest reduction in emission, despite having by far the greatest magnitude of surface forcing (Table 1). Although we have focused on the relation between emission and forcing at the surface, we note that the relation is no more apparent if forcing at the top of the atmosphere (TOA) is considered.

Figure 5d shows that the relationship between the annual averages of surface forcing and the emission anomaly is only approximately linear, even though emission is generally reduced in all experiments that include this forcing. The limited relation between surface forcing and emission is not improved even if regression is performed on averages as short as a month. The poor correspondence is consistent with the findings of Perlwitz *et al.* [2001], where emission is more highly correlated with monthly average wind speed than the speed formed by the monthly average components of the surface wind. Time scales shorter than a month contribute to the correlation only for the former.

We consider whether there are shorter time scales in

which the relationship between the forcing and surface wind is apparent. Because of the strongly non-linear relation between emission and wind speed, competing effects of the radiative forcing upon emission on short time scales may result in an emission anomaly on seasonal time scales that is poorly correlated with seasonal variations of wind speed. Because of the prominence of the diurnal cycle of dust emission at some of the most productive sources (Figures 3 and 4), we examine the relation between forcing, surface wind speed, and emission at this time scale. Figure 6 shows the variation of various physical quantities over the course of a typical day for the Australian location (Figures 3b and 4b). The cycle represents an average over the Southern Hemisphere summer season (DJF) when emission and forcing are largest at this location. (The forcing is given in Table 2.)

Over the Australian desert, the surface flux of sensible heat increases sharply after sunrise and peaks in the early afternoon (Figure 6d). The transport of heat away from the surface, which partly compensates the incident sunlight, is reduced by the aerosol layer overhead, with the largest reduction for the experiment with more absorbing particles ( $0.9 \times \varpi$ ), as in Figure 5. In response to this heating, the boundary layer deepens throughout the morning (not shown), while the turbulent kinetic energy and vertical viscosity increase (Figure 7a,c). Momentum from the faster winds aloft is mixed toward the surface, causing an increase in surface drag and wind speed (Figures 6b and c). Dust emission increases sharply after sunrise (Figure 6d), until its marked reduction in the late morning. During the morning, the acceleration of the surface wind is reduced in proportion to the surface radiative forcing, causing a corresponding reduction in emission. Figures 6c and d are clear evidence that dust radiative forcing reduces emission and the surface wind by decreasing mixing within the PBL.

The total daily emission and its dependence upon surface forcing cannot be understood solely in terms of the morning behavior. During the late afternoon the largest surface wind stress and emission over Australia occur for the most absorbing particles ( $0.9 \times \varpi$ ), even though the surface heat flux that drives the boundary layer is smallest in this case. Because of this contrasting dependence between morning and afternoon, the diurnal average of emission does not fall uniformly with increasing surface forcing (Figure 6d).

The afternoon increase in wind speed and emission in the experiment with more absorbing particles ( $0.9 \times \varpi$ ) can be explained partly by the relation at the surface between wind speed  $u_s$  and wind stress magnitude  $\tau_s = C_{DM}u_s^2$ , where  $C_{DM}$  is the surface drag coefficient. This coefficient is an increasing function of the surface sensible heat flux [Hartke and Rind, 1997]. For a given surface wind stress, the wind speed  $u_s$  increases with the magnitude of the surface forcing, which reduces the heat flux and thus  $C_{DM}$ .

The morning peak in emission, and its reduction in proportion to dust radiative forcing, is exhibited in Central Asia (Figure 8b), another productive source location. In contrast, the morning reduction in surface wind speed and emission is nearly independent of the surface forcing at a prolific source in the western Sahara (Table 2, Figure 8d). At this location, the reduction of the surface sensible heat flux anomaly does not vary strongly with the forcing (not shown). Consequently, variations of vertical mixing between the experiments with dust radiative forcing are small (not shown). We note that the weak relation at this location between the sensible heat flux and the forcing is exceptional. These two variables

are in general highly correlated, as shown in Figure 5b and Table 3.

At the most productive sources, mixing is consistently reduced in proportion to the surface radiative forcing. Figures 9a and b regress forcing against the turbulent viscosity  $\nu_M$  at the top and base of the boundary layer. That the strength of the regression varies with height indicates that the feedback depends upon the vertical dependence of the perturbation to mixing by dust radiative forcing, which may vary among AGCM turbulence parameterizations. Vertical mixing is even more highly correlated with the surface sensible heat flux (Figures 9c and d) than the surface radiative forcing. This difference can be attributed to the imprecise (albeit high) correlation of the forcing and heat flux (Figure 5b).

Despite the strengthening of the surface winds following sunrise at all locations, the diurnal cycle of surface wind speed never exceeds the threshold for emission listed in Table 2. This is consistent with the sporadic nature of observed emission. While emission is favored during certain times of the day, when the surface winds are strongest, day to day wind fluctuations are required to augment the mean diurnal cycle.

Whether the model feedback between dust radiative forcing and emission can be observed depends upon the realism of the AGCM. We compare observations taken near the most prolific dust sources to assess the model's diurnal cycle of surface wind speed. The comparison is not entirely appropriate as the AGCM value represents a spatial average over the extent of the grid box rather than the value observed at a single location. Moreover, the crude AGCM representation of topography means that the model is more capable of reproducing the atmospheric circulation at continental scales than local winds, which reflect intricate variations in elevation and the land surface. Figure 10 compares the AGCM winds to observed values at the three most prolific dust sources in the model. In all locations, the diurnal cycle of surface wind speed in the AGCM is too small, compared to its daily average. In addition, the AGCM values over the Australian and western Sahara sources decelerate too rapidly after mid-morning, falling to a relative minimum within a few hours, rather than declining gradually throughout the afternoon as observed. These discrepancies suggest that the change in the diurnal cycle by dust radiative forcing is underestimated by the AGCM. Moreover, the rapid deceleration after late-morning may exaggerate the semi-diurnal harmonic of emission (Figure 3).

The observed morning acceleration of the surface wind is not particular to our three stations, but has been observed in terrain ranging from the continental interior of Australia and the American Great Plains to a maritime location in Denmark [*Crawford and Hudson, 1973; Mahrt, 1981*]. At many locations, surface wind speed is observed to increase with the surface heat flux until just after midday, as illustrated by the Central Asia station. The sharp decrease in AGCM wind speed after mid-morning occurs despite increasingly vigorous mixing until the decline of the surface heat flux in the mid afternoon (Figure 7a). A more recent PBL parameterization within the GISS AGCM [*Cheng et al., 2002*] results in strong daytime winds that persist throughout the early afternoon.

The rapid deceleration of the model surface wind after mid-morning may distort the AGCM feedback of surface radiative forcing upon emission. As mixing within the PBL strengthens after sunrise, surface radiative forcing by dust reduces the acceleration of the surface wind (Figure 6c). In the model, this dependence is offset by con-

trasting behavior in the afternoon. Were the strong daytime surface wind to persist in the AGCM as observed, the reduction of emission with surface forcing would be exhibited over a greater fraction of the day. The decrease of wind speed and emission with surface forcing might be more apparent in the diurnal (and seasonal) average, despite the offsetting effect of the surface drag coefficient.

As noted above, the AGCM surface wind speed represents an average over the spatial extent of the grid box and the duration of each model time step. Fluctuations at higher frequencies and smaller spatial scales are not included. *Cakmur et al.* [2004] parameterize the emission due to these fluctuations. The greatest contribution comes from dry convective eddies, which are observed to vary with the surface flux of sensible heat [*Stull*, 1988]. We are currently introducing this parameterization into the GISS AGCM. By reducing the sensible heat flux, dust radiative forcing is expected to further reduce emission by this mechanism, especially over the Sahara and Taklimakan deserts, where wind fluctuations that are not explicitly resolved have the greatest effect upon emission [*Cakmur et al.*, 2004].

In the current version of the AGCM, emission depends upon prescribed geographic variations in the threshold wind speed. After linearizing the relation (1) between emission  $\mathcal{E}$  and surface wind speed  $u_s$ , the anomaly created by dust radiative forcing is:

$$\delta\mathcal{E} = 2C\bar{u}_s(\bar{u}_s - u_T)\delta u_s + C\bar{u}_s^2\delta u_s, \quad (2)$$

where  $\delta$  denotes the anomaly created by radiative forcing and  $\bar{u}_s$  is the unperturbed wind speed. The contribution to the emission anomaly by the first term on the right-hand side depends upon the proximity of the unperturbed wind to the threshold. This suggests that geographic variations of the emission threshold  $u_T$  introduce corresponding variations in the feedback between dust radiative forcing and emission. These variations may change if a more physical representation of subgrid wind variations is used.

While the effect of dust radiative forcing is apparent in the vigor of daytime mixing, dust has the potential to alter the emission at night, when the observed surface wind is generally weak (Figure 10). The reduced mixing of momentum to the surface is partly a consequence of the increased stability of the boundary layer after sundown, when the surface cools by emitting longwave radiation. By absorbing and reemitting longwave radiation back toward the surface, dust has the potential to extend the mixing and delay the surface deceleration. In the present AGCM, the reduction of the net upward flux of longwave by dust is small compared to the solar reduction, and variations in surface wind and emission between the experiments at night are small (Figure 6c,d). However, the effective radius of the largest particles in our model is  $4\ \mu\text{m}$ , too small to trap longwave efficiently in the spectral window at roughly  $10\ \mu\text{m}$ , where absorption by water vapor and carbon dioxide is weak. Particles with  $10\ \mu\text{m}$  radii are observed in the vicinity of dust storms [*Gillies et al.*, 1996], and by modeling this size explicitly, *Tegen et al.* [2002] show that they dominate the particle size distribution in the vicinity of sources. These large particles that effectively trap longwave radiation settle rapidly, and have little effect upon the global radiative budget due to their short trajectories. However, their large radiative forcing near the source area can alter emission, even of the smaller particles that travel thousands of kilometers downwind and contribute predominately to the global forcing.

## 5. Conclusions

*Perlwitz et al.* [2001] calculate dust emission in an AGCM in which dust radiative forcing alters the model climate, in turn feeding back upon emission. The inclusion of dust radiative forcing reduces annual emission by roughly 15% compared to an experiment omitting this forcing. Here, we interpret this reduction in terms of the interaction between dust radiative forcing and the planetary boundary layer.

At some of the most productive sources of dust aerosol in the AGCM, emission has a prominent diurnal cycle related to daily development of the planetary boundary layer. By reducing sunlight incident upon the surface, dust reduces the turbulent flux of sensible heat back into the atmosphere. Because this flux drives mixing within the boundary layer, dust radiative forcing reduces the downward transport of momentum from the relatively fast winds aloft, thus decreasing the surface wind speed, along with dust emission. We illustrate this feedback at a grid box within the Australian outback, where mixing intensifies following sunrise and the surface wind accelerates. At this location, the reduction in emission increases with the magnitude of the surface radiative forcing.

This negative feedback is exhibited in an AGCM simulation of the Martian atmosphere [*Newman et al.*, 2002], where emission is explicitly parameterized in terms of the surface sensible heat flux. In contrast, we show that this same feedback emerges naturally in our AGCM, given conventional parameterizations of emission as a function of wind speed, and an explicit representation of turbulent transport within the PBL.

While this negative feedback is apparent in the initial development of the PBL each morning, there is a second feedback with a different dependence upon surface radiative forcing that is apparent in the afternoon. Here, for a given wind stress, the wind speed increases with magnitude of the surface forcing, because the surface drag coefficient decreases with the surface heat flux. Note that this feedback is an artifact of our formulation of dust emission in terms of the surface wind speed. Were the formulation based upon surface wind stress, as suggested by physical considerations and wind tunnel measurements, this feedback would be absent. When the morning and afternoon feedbacks are considered separately, the relation between forcing and emission is clear. However, the relationship is obscured by averaging over the diurnal cycle (Figure 6d). This reflects the highly non-linear behavior of parameterizations of both the planetary boundary layer and dust emission.

This non-linearity makes it difficult to identify mechanisms relating forcing and emission, and our assessment has been more exploratory than exhaustive. We have attempted to generalize the behavior seen at a few grid boxes by correlating annual averages of surface radiative forcing and emission at the thirty most prolific sources in our model (that together account for two-thirds of the global emission). The correlation is marginally significant (Table 3). A higher correlation may be precluded by the diurnal averaging associated with the annual means, which bundles together feedbacks with conflicting dependencies upon the forcing, as described above. Alternatively, the modest correlation may result from other mechanisms that we have yet to identify. At some prolific sources, like the eastern Sahara grid box (Figure 4d), the interaction between dust radiative forcing and the diurnal cycle of the PBL that we find elsewhere does not apply. Here, the diurnal cycle of emission is prominent, but is hardly altered by dust radiative forcing.

The complicated physical interactions comprising the feedback make it difficult to anticipate whether the reduction in emission found by *Perlwitz et al.* [2001] is generic and likely to be exhibited to the same degree by other models. Vertical mixing within the PBL is central to this feedback. Although mixing is reduced in proportion to the magnitude of dust radiative forcing at all locations we examined, this dependence is smallest at the base of the boundary layer (Figure 9). This demonstrates that the feedback upon emission may depend upon details in the vertical distribution of boundary layer mixing, which may vary from model to model and be difficult to evaluate with observations.

We suggest that the morning feedback might be more dominant than indicated by our model, so that the actual reduction in emission might scale more simply with the surface forcing. At the two most productive source regions — the Western Sahara and Australian outback — the surface wind stress and wind speed fall off sharply after the mid-morning despite the increase of turbulent kinetic energy and momentum mixing within the PBL until the late afternoon. This rapid deceleration of the surface wind, despite strong vertical mixing, is contrary to observations. Were the surface winds in our model to remain in proportion to vertical mixing throughout the day, the acceleration of the surface wind in inverse proportion to the surface radiative forcing might be the dominant feedback.

In our model, the surface wind speed used to calculate emission represents an average over the duration of the model time step and the extent of the grid box. The effect of wind speed fluctuations on smaller and more rapid time scales is neglected. These fluctuations have been parameterized by *Cakmur et al.* [2004], who show that convective eddies increase dust emission preferentially over deserts like the Sahara and Taklimakan in western China. Observations and modeling suggest that convective fluctuations in surface wind speed vary with the surface heat flux. By decreasing the energy available to dry convective eddies, dust radiative forcing should reduce the wind speed fluctuations that emit dust. We are implementing this effect in our model, and expect this to increase the reduction in emission for a given value of the surface forcing.

Our focus upon the PBL suggests interactions with dust that are currently not simulated by the AGCM. In our model, dust is deposited onto the surface by turbulence with a settling speed that does not increase with the intensity of PBL mixing [*Tegen and Fung, 1994*]. We are currently introducing this dependence to our model, allowing dust radiative forcing to increase the dust lifetime even as the emission is reduced. We also suggest that large particles of radius  $10\ \mu\text{m}$ , although unimportant to the global radiative budget due to their short lifetime, could greatly increase the longwave forcing by absorbing within the spectral window of water vapor and carbon dioxide. This reduces nocturnal cooling at the surface, maintaining mixing and the large daytime surface wind within the PBL past sundown. In addition, downward emission of longwave by large particles offsets the reduction of sunlight at the surface by dust, especially in the afternoon, when the boundary layer is warmest. With enough large particles, the net forcing into the surface could even become positive [*Liao and Seinfeld, 1998; Claquin et al., 1998*], increasing the sensible heat flux into the atmosphere and boundary layer mixing, leading to a positive feedback upon dust emission. Larger particles, although not important globally, may feed back upon the emission of the smallest particles that are transported

worldwide and make the largest contribution to global radiative forcing.

#### Acknowledgments.

This article was improved by the comments of Natalie Mahowald and an anonymous reviewer. We also thank Brian Cairns, Paul Ginoux, David Rind, and Reto Ruedy for their expertise. This work was supported by the Climate Dynamics Program of the National Science Foundation through ATM-97-27872.

## Notes

1. While *Hartke and Rind* [1997] ostensibly describe the parameterization of vertical momentum transport in a previous version of the AGCM, the more accurate second-order closure scheme used here is also described.

## References

- Alfaro, S. C., and L. Gomes (2001), Modeling mineral aerosol production by wind erosion: Emission intensities and aerosol size distributions in source areas., *J. Geophys. Res.*, *106*, 18,075–18,084.
- Arya, S. P. (1988), *Introduction to Micrometeorology*, Academic Press, San Diego, 307 pp.
- Biscaye, P. E., F. E. Grousset, M. Revel, S. van der Gaast, G. A. Zielinski, A. Vaars, and G. Kukla (1997), Asian provenance of glacial dust (stage 2) in the Greenland Ice Sheet Project 2 Ice Core, Summit, Greenland, *J. Geophys. Res.*, *102*, 26,765–26,781.
- Burpee, R. W. (1972), The origin and structure of easterly waves in the lower troposphere of North Africa, *J. Atmos. Sci.*, *29*, 77–90.
- Cakmur, R., R. L. Miller, and O. Torres (2004), Incorporating the effect of small-scale circulations upon dust emission in an atmospheric general circulation model, *J. Geophys. Res.*, *109*, D07201, doi:10.1029/2003JD4067.
- Carlson, T. N., and J. M. Prospero (1972), The large-scale movement of Saharan air outbreaks over the northern equatorial Atlantic, *J. Appl. Meteorol.*, *11*, 283–297.
- Cheng, Y., V. M. Canuto, and A. M. Howard (2002), An improved model for the turbulent PBL, *J. Atmos. Sci.*, *59*, 1550–1565, doi:10.1175/1520-0469(2002)059<1550:AIMFTT>2.0.CO;2.
- Claquin, T., M. Schulz, Y. Balkanski, and O. Boucher (1998), Uncertainties in assessing radiative forcing by mineral dust, *Tellus*, *50B*, 491–505.
- Crawford, K. C., and H. R. Hudson (1973), The diurnal wind variation in the lowest 1500 feet in Central Oklahoma: June 1966–May 1967, *J. Appl. Meteorol.*, *12*, 127–132.
- Druyan, L., and T. M. Hall (1994), Studies of African wave disturbances with the GISS GCM, *J. Climate*, *7*, 261–276.
- Dubovik, O., B. N. Holben, T. F. Eck, A. Smirnov, Y. J. Kaufman, M. D. King, D. Tanre, and I. Slutsker (2002), Variability of absorption and optical properties of key aerosol types observed in worldwide locations, *J. Atmos. Sci.*, *59*, 590–608.
- Dufresne, J.-L., C. Gautier, R. P., and Y. Fouquart (2002), Longwave scattering effects of mineral aerosols, *J. Atmos. Sci.*, *59*, 1959–1966.
- Galperin, B., L. H. Kantha, S. Hassid, and A. Rosatti (1988), A quasi-equilibrium turbulent energy model for geophysical flows, *J. Atmos. Sci.*, *45*, 55–62.
- Gillies, J. A., W. G. Nickling, and G. H. McTainsh (1996), Dust concentrations and particle-size characteristics of an intense dust haze event: Inland delta region, Mali, West Africa, *Atmos. Environ*, *30*, 1081–1090.
- Ginoux, P., M. Chin, I. Tegen, J. Prospero, B. Holben, O. Dubovik, and S. J. Lin (2001), Sources and distributions of aerosols simulated with the GOCART model, *J. Geophys. Res.*, *106*, 20,255–20,273.
- Hansen, J., M. Sato, L. Nazarenko, R. Ruedy, et al. (2002), Climate forcings in Goddard Institute for Space Stud-

- ies SI2000 simulations, *J. Geophys. Res.*, *107*, 4347, doi:10.1029/2001JD001143.
- Hartke, G., and D. Rind (1997), Improved surface and boundary layer models for the Goddard Institute for Space Studies general circulation model, *J. Geophys. Res.*, *102*, 16,407–16,422.
- Herman, J. R., P. K. Bhartia, O. Torres, C. Hsu, C. Seftor, and E. Celarier (1997), Global distribution of UV-absorbing aerosols from Nimbus-7/TOMS data, *J. Geophys. Res.*, *102*, 16,911–16,922.
- Husar, R. B., J. M. Prospero, and L. L. Stowe (1997), Characterization of tropospheric aerosols over the oceans with the NOAA advanced very high resolution radiometer optical thickness operational product, *J. Geophys. Res.*, *102*, 16,889–16,909.
- Jones, C., N. Mahowald, and C. Luo (2003), The role of Easterly waves in African dust transport, *J. Climate*, *16*, 3617–3628.
- Kahn, R. A., T. Z. Martin, and R. W. Zurek (1992), *Mars*, chap. 29. The Martian Dust Cycle, p. 1536, U. Arizona Press, Tuscon.
- Kaufman, Y. J., D. Tanré, O. Dubovik, A. Karnieli, and L. A. Remer (2001), Absorption of sunlight by dust as inferred from satellite and ground-based remote sensing, *Geophys. Res. Lett.*, *28*, 1479–1482.
- Lacis, A. A., and M. I. Mishchenko (1995), Climate forcing, climate sensitivity, and climate response: a radiative modeling perspective on atmospheric aerosols, in *Aerosol Forcing of Climate*, edited by R. J. Charlson and J. Heintzenberg, chap. 2, pp. 11–42, John Wiley and Sons Ltd.
- Liao, H., and J. H. Seinfeld (1998), Radiative forcing by mineral dust aerosols: sensitivity to key variables, *J. Geophys. Res.*, *103*, 31,637–31,645.
- Luo, C., N. Mahowald, and C. Jones (2004), Temporal variability of dust mobilization and concentration in source regions, *J. Geophys. Res.*, (submitted).
- Mahrt, L. (1981), The early evening boundary layer transition, *Q. J. R. Met. Soc.*, *107*, 329–343.
- Matthews, E. (1983), Global vegetation and land use: New high-resolution data bases for climate studies, *J. Clim. Appl. Meteorol.*, *22*, 474–487.
- Mellor, G. L., and T. Yamada (1982), Development of a turbulent closure model for geophysical fluid problems, *Rev. Geophys. and Space Phys.*, *20*, 851–875.
- Miller, J. R., G. L. Russell, and L.-C. Tsang (1983), Annual oceanic heat transports computed from an atmospheric model, *Dyn. Atmos. & Oceans*, *7*, 95–109.
- Miller, R. L., and I. Tegen (1998), Climate response to soil dust aerosols, *J. Climate*, *11*, 3247–3267.
- Miller, R. L., and I. Tegen (1999), Radiative forcing of a tropical direct circulation by soil dust aerosols, *J. Atmos. Sci.*, *56*, 2403–2433.
- Miller, R. L., J. Perlwitz, and I. Tegen (2004a), Modeling Arabian dust mobilization during the Asian summer monsoon: the effect of prescribed versus calculated SST, *Geophys. Res. Lett.*, (accepted).
- Miller, R. L., I. Tegen, and J. Perlwitz (2004b), Surface radiative forcing by soil dust aerosols and the hydrologic cycle, *J. Geophys. Res.*, *109*, D04203, doi:10.1029/2003JD004085.
- Newman, C. E., S. R. Lewis, and P. L. Read (2002), Modeling the Martian dust cycle, 1, Representations of dust transport processes, *J. Geophys. Res.*, *107*(E12), 5123, doi:10.1029/2002JE001910.
- N’Tchayi Mbourou, G., J. Bertrand, and S. Nicholson (1997), The diurnal and seasonal cycles of wind-borne dust over Africa North of the Equator, *J. Appl. Meteorol.*, *36*, 868–882.
- Patterson, E. M., D. A. Gillette, and B. H. Stockton (1977), Complex index of refraction between 300 and 700 nm for Saharan aerosols, *J. Geophys. Res.*, *82*, 3153–3160.
- Perlwitz, J., I. Tegen, and R. L. Miller (2001), Interactive soil dust aerosol model in the GISS GCM. Part I: Sensitivity of the soil dust cycle to radiative properties of soil dust aerosols, *J. Geophys. Res.*, *106*, 18,167–18,192.
- Prather, M. (1986), Numerical advection by conservation of second-order moments, *J. Geophys. Res.*, *91*, 6671–6680.

- Press, W. H., S. A. Teukolsky, W. T. Vetterling, and B. P. Flannery (1992), *Numerical Recipes in Fortran 77: The Art of Scientific Computing*, second ed., Cambridge University Press, New York, USA.
- Prospero, J. M., and P. J. Lamb (2003), African droughts and dust transport to the Caribbean: climate change implications, *Science*, *302*, 1024–1027.
- Prospero, J. M., R. A. Glaccum, and R. T. Nees (1981), Atmospheric transport of soil dust from Africa to South America, *Nature*, *289*, 570–572.
- Prospero, J. M., P. Ginoux, O. Torres, and S. Nicholson (2002), Environmental characterization of global sources of atmospheric soil dust derived from NIMBUS-7 TOMS absorbing aerosol product, *Rev. Geophys.*, *40*, doi:10.1029/2000RG000095.
- Rea, D. K. (1994), The paleoclimatic record provided by eolian deposition in the deep sea: The geologic history of wind, *Rev. Geophys.*, *32*, 159–195.
- Read, P. L., and S. R. Lewis (2004), *The Martian Climate Revisited: Atmosphere and Environment of a Desert Planet*, Springer-Verlag, Berlin, 330 p.
- Shao, Y. (2000), *Physics and Modelling of Wind Erosion*, Kluwer Academic, xXXp.
- Shao, Y., M. R. Raupach, and P. A. Findlater (1993), Effect of saltation bombardment on the entrainment of dust by wind, *J. Geophys. Res.*, *98*, 12,719–12,726.
- Sinyuk, A., O. Torres, and O. Dubovik (2003), Combined use of satellite and surface observations to infer the imaginary part of the refractive index of Saharan dust, *Geophys. Res. Lett.*, *30*, doi:10.1029/2002GL016189.
- Sokolik, I., A. Andronova, and T. C. Johnson (1993), Complex refractive index of atmospheric dust aerosols, *Atmos. Env.*, *27A*, 2495–2502.
- Stull, R. B. (1988), *An Introduction to Boundary Layer Meteorology*, Kluwer Academic, Boston, 666p.
- Tegen, I., and I. Fung (1994), Modeling of mineral dust in the atmosphere: Sources, transport, and optical thickness, *J. Geophys. Res.*, *99*, 22,897–22,914.
- Tegen, I., and A. A. Lacis (1996), Modeling of particle influence on the radiative properties of mineral dust aerosol, *J. Geophys. Res.*, *101*, 19,237–19,244.
- Tegen, I., and R. Miller (1998), A general circulation model study on the interannual variability of soil dust aerosol, *J. Geophys. Res.*, *103*, 25,975–25,995.
- Tegen, I., S. P. Harrison, K. Kohfeld, I. C. Prentice, C. M., and M. Heimann (2002), The impact of vegetation and preferential source areas on global dust aerosol: Results from a model study, *J. Geophys. Res.*, *107*, 4576, doi:10.1029/2002JD002365.
- van de Hulst, H. C. (1957), *Light Scattering by Small Particles*, Dover, New York, 470 pp.
- Volz, F. E. (1973), Infrared optical constants of ammonium sulfate, Sahara dust, volcanic pumice and flyash, *Appl. Optics*, *12*, 564–568.
- Welch, P. D. (1967), The use of fast Fourier transform for the estimation of power spectra: A method based upon time averaging over short, modified periodograms., *IEEE Trans. Audio and Electroacoust.*, *AU-15*, 70–73.
- Westphal, D. L., O. B. Toon, and T. N. Carlson (1988), A case study of mobilization and transport of Saharan dust, *J. Atmos. Sci.*, *45*, 2145–2175.
- Yu, H., S. C. Liu, and R. E. Dickinson (2002), Radiative effects of aerosols on the evolution of the atmospheric boundary layer, *J. Geophys. Res.*, *107*, doi:10.1029/2001JD000754.
- Zender, C. S., H. Bian, and D. Newman (2003a), The mineral Dust Entrainment And Deposition (DEAD) model: description and 1990's dust climatology, *J. Geophys. Res.*, *108*, 4416, doi:10.1029/2002JD002775.
- Zender, C. S., D. Newman, and O. Torres (2003b), Spatial heterogeneity in aeolian erodibility: uniform, topographic, geomorphic, and hydrologic hypotheses, *J. Geophys. Res.*, *108*, 4543, doi:10.1029/2002JD003039.

---

R. L. Miller, Dept. of Applied Physics and Applied Math, Columbia University, 2880 Broadway, New York, NY 10025. (rlm15@columbia.edu).

J. Perlwitz, Dept. of Applied Physics and Applied Math,  
Columbia University, 2880 Broadway, New York, NY 10025.  
(jp544@columbia.edu).

I. Tegen, Max-Planck-Institut für Biogeochemie, Postfach  
100164, 07701 Jena, Germany. (itegen@bgc-jena.mpg.de).

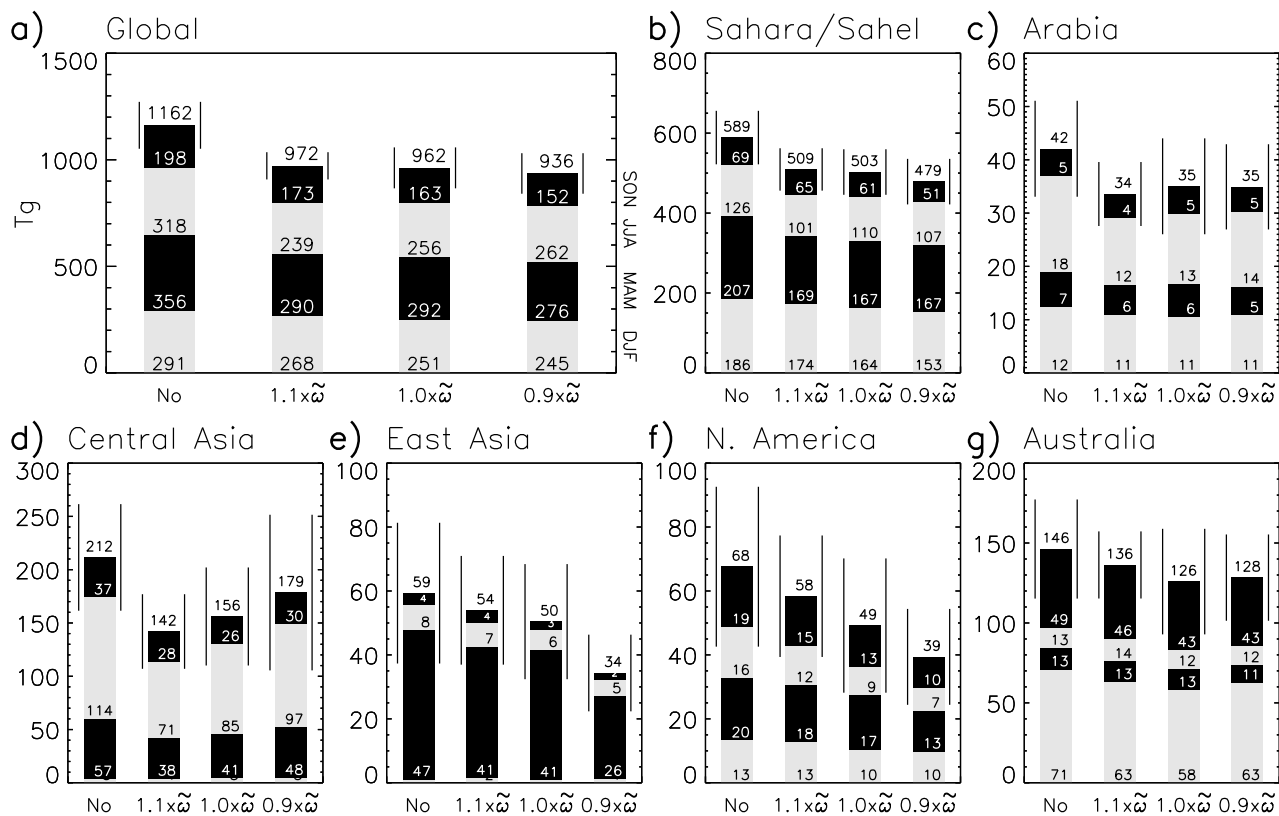


**Figure 1.** Global and regional emission of soil dust aerosol (Tg), as calculated by each experiment. The experiment omitting dust radiative forcing is denoted by ‘No’, while the experiments including forcing are denoted by  $1.0 \times \tilde{\omega}$ ,  $0.9 \times \tilde{\omega}$ , and  $1.1 \times \tilde{\omega}$  for baseline, more absorbing, and more reflecting particles, respectively. Each bar is divided into seasonal averages for DJF (bottom, light), MAM (above, dark), JJA, (above, light), and SON (top, dark). The annual average is given at the top of each bar. The vertical lines bracketing the annual average range between one standard deviation above and below. The Sahara/Sahel regional average is based upon Northern Hemisphere Africa gridboxes. Central Asia is defined between 25–90°E, 36–56°N; East Asia between 90–140°E, 32–52°N; and Arabia between 35–60°E (but east of the Red Sea) and 12–36°N.

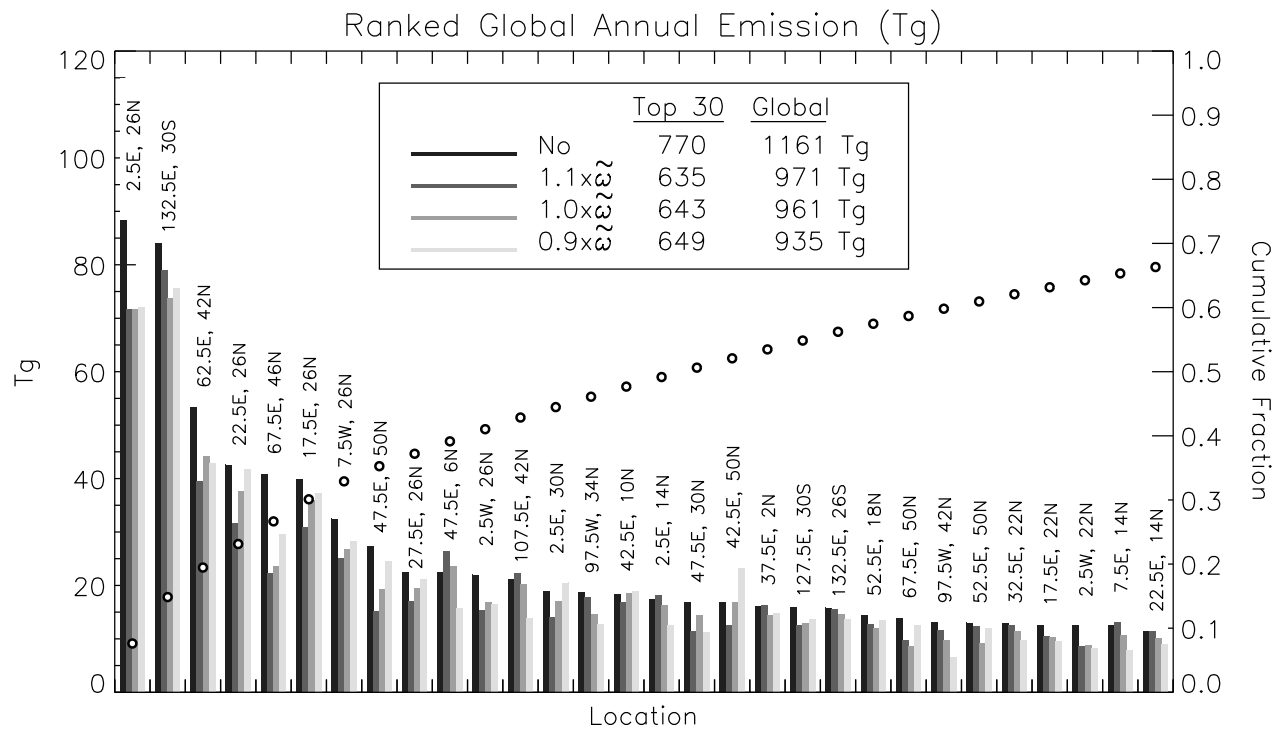


**Figure 2.** Annual mean emission ranked by location for the experiment excluding dust radiative effects (darkest bar). Progressively lighter bars at each location show emission for the experiments with more reflecting particles ( $1.1 \times \tau$ ), baseline particles ( $1.0 \times \tau$ ), and more absorbing particles ( $0.9 \times \tau$ ), respectively. The circles show the cumulative fraction of global emission for the most productive emitting locations in the experiment excluding dust radiative forcing. (e.g., the 30 most productive locations account for two-thirds of the global annual total.) In the inset, the two columns list the cumulative sum in Tg for the top 30 gridboxes along with the global total for each experiment.

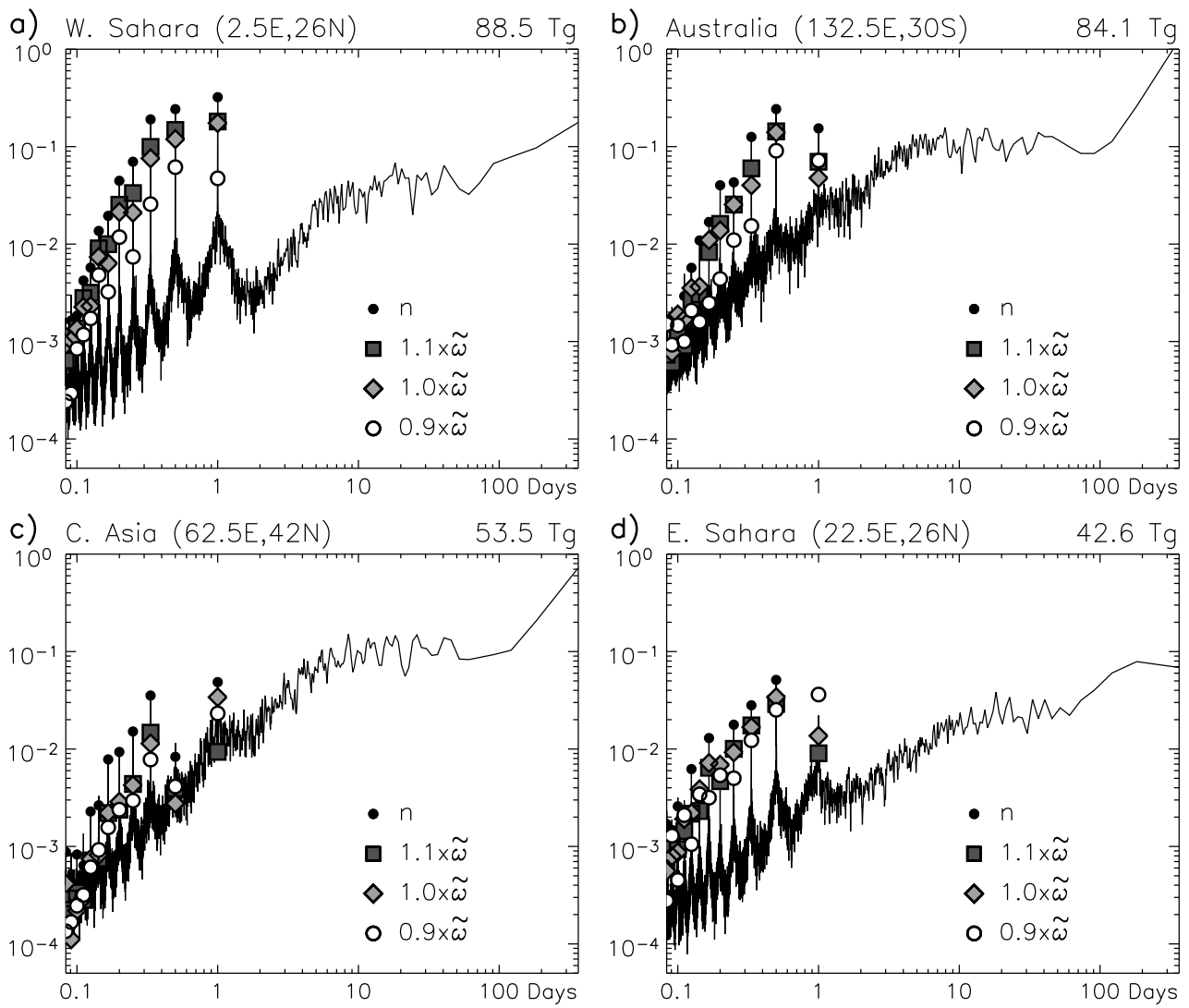


**Figure 3.** Power spectrum of ten years of hourly AGCM emission at the four most productive emitting sites in the experiment omitting dust radiative forcing. The power spectrum (vertical axis) has units of  $\text{g}^2 \text{m}^{-4} \text{d}^{-2}$ . The diurnal harmonics are marked by filled circles. At the diurnal harmonics, power is also shown for the experiments with more reflecting particles ( $1.1 \times \varpi$ , squares), baseline particles ( $1.0 \times \varpi$ , diamonds), and more absorbing particles ( $0.9 \times \varpi$ , open circles). The mean annual emission is listed at the upper right corner.

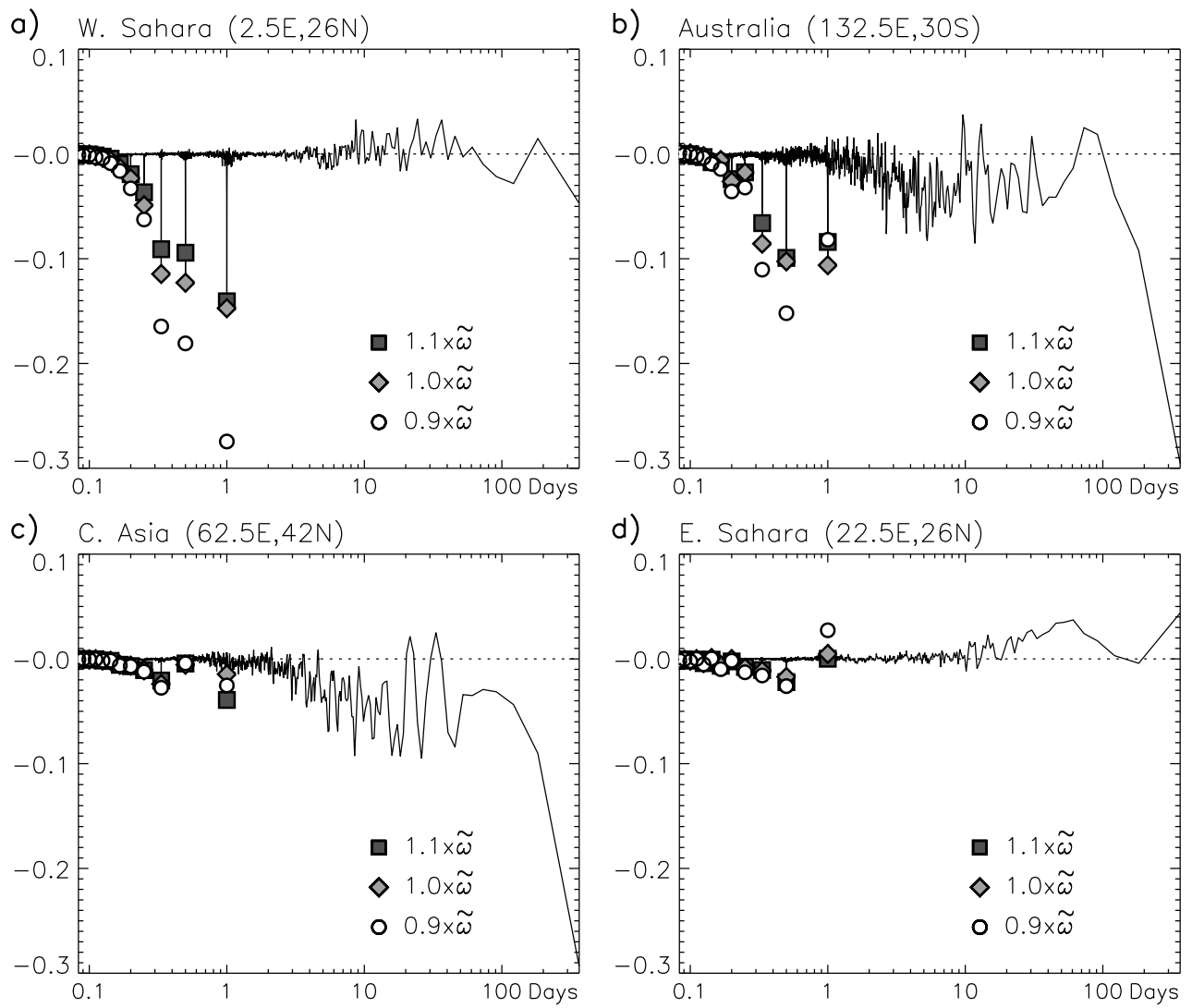


**Figure 4.** Difference between emission spectra (in  $\text{g}^2 \text{m}^{-4} \text{d}^{-2}$ ) for the baseline experiment ( $1.0 \times \varpi$ ) with dust radiative forcing and the experiment omitting this forcing at the locations shown in Figure 3. The diurnal harmonics are marked by diamonds. At diurnal harmonics, the difference is also shown for the experiments with more reflecting ( $1.1 \times \varpi$ , squares) and absorbing particles ( $0.9 \times \varpi$ , open circles).

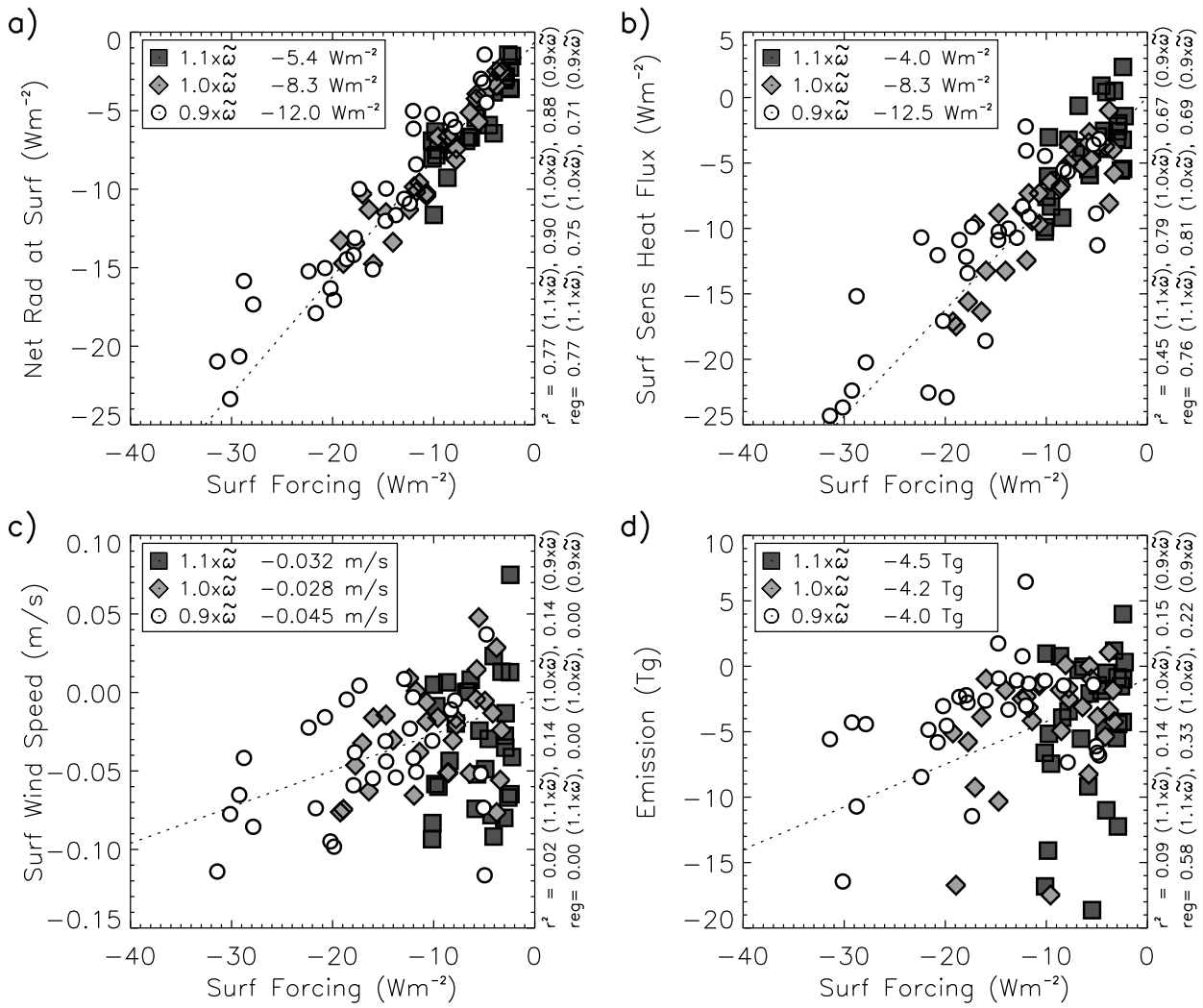


**Figure 5.** Regression of dust radiative forcing at the surface with respect to anomalies of a) net downward radiation into the surface, b) sensible heat flux from the surface to the atmosphere, c) surface wind speed, and d) dust emission. The anomalies are with respect to the control experiment that calculates a dust cycle but omits its radiative forcing. Annual averages are plotted, which allows source regions that emit at different times of the year to be summarized in a single figure. The regression is carried out at the thirty grid boxes with the largest annual emission (identified in Figure 2, based upon the experiment omitting dust radiative forcing). The experiments with radiative forcing are marked by squares ( $1.1 \times \varpi$ , more reflecting particles), diamonds ( $1.0 \times \varpi$ , baseline particles), and circles ( $0.9 \times \varpi$ , more absorbing particles). The regression line for the baseline experiment is dotted. ‘reg’ and ‘ $r^2$ ’ give for each experiment the regression slope and variance accounted for by the regression line. The box within each panel lists for each experiment the average anomaly for the thirty locations.

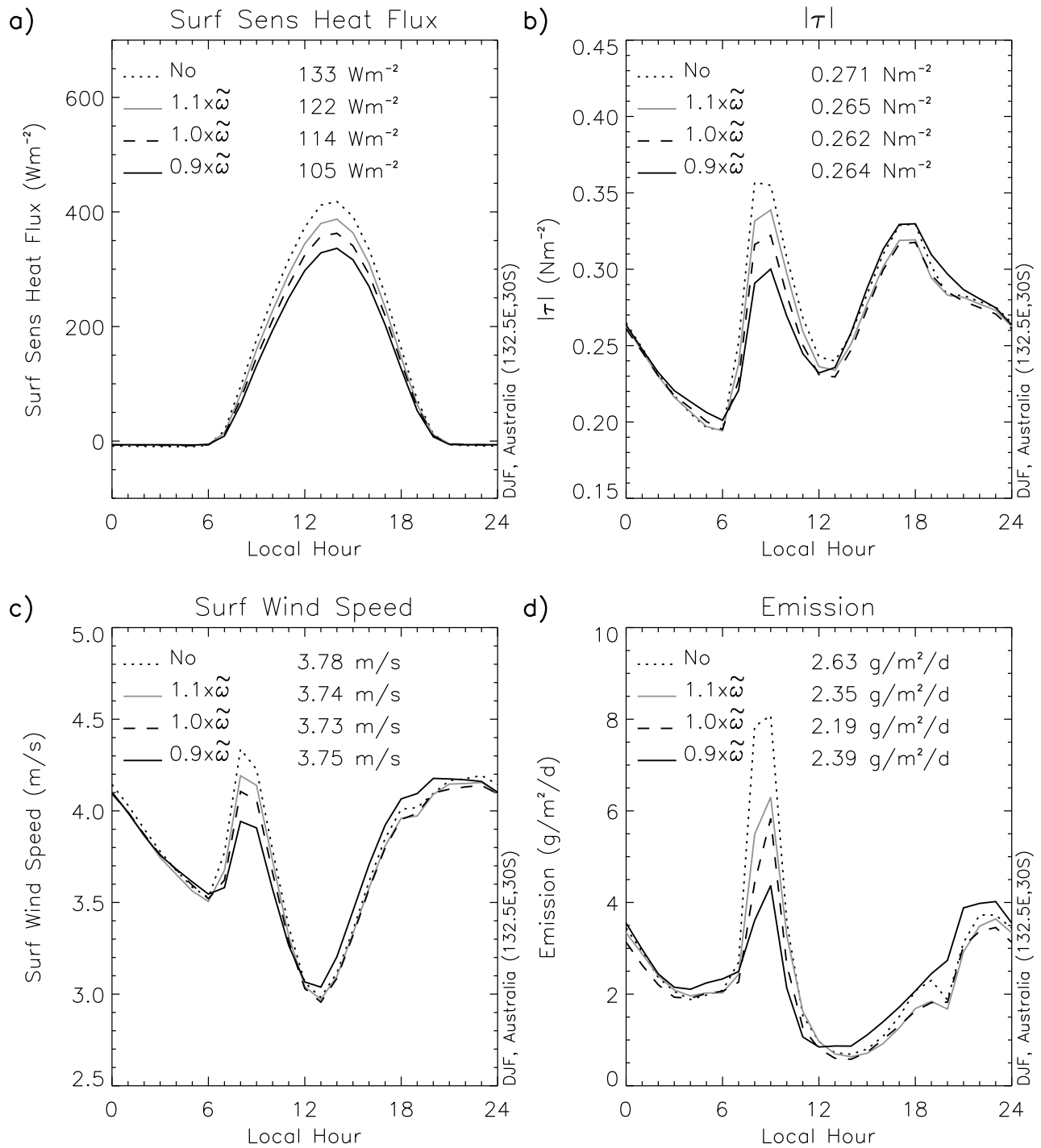


**Figure 6.** DJF diurnal cycle of a) surface sensible heat flux into the atmosphere, b) surface wind stress magnitude, c) surface wind speed, and d) dust emission, at the Australian desert source identified in Figure 3b. Diurnal averages for each experiment are listed in the upper-right corner of each panel.

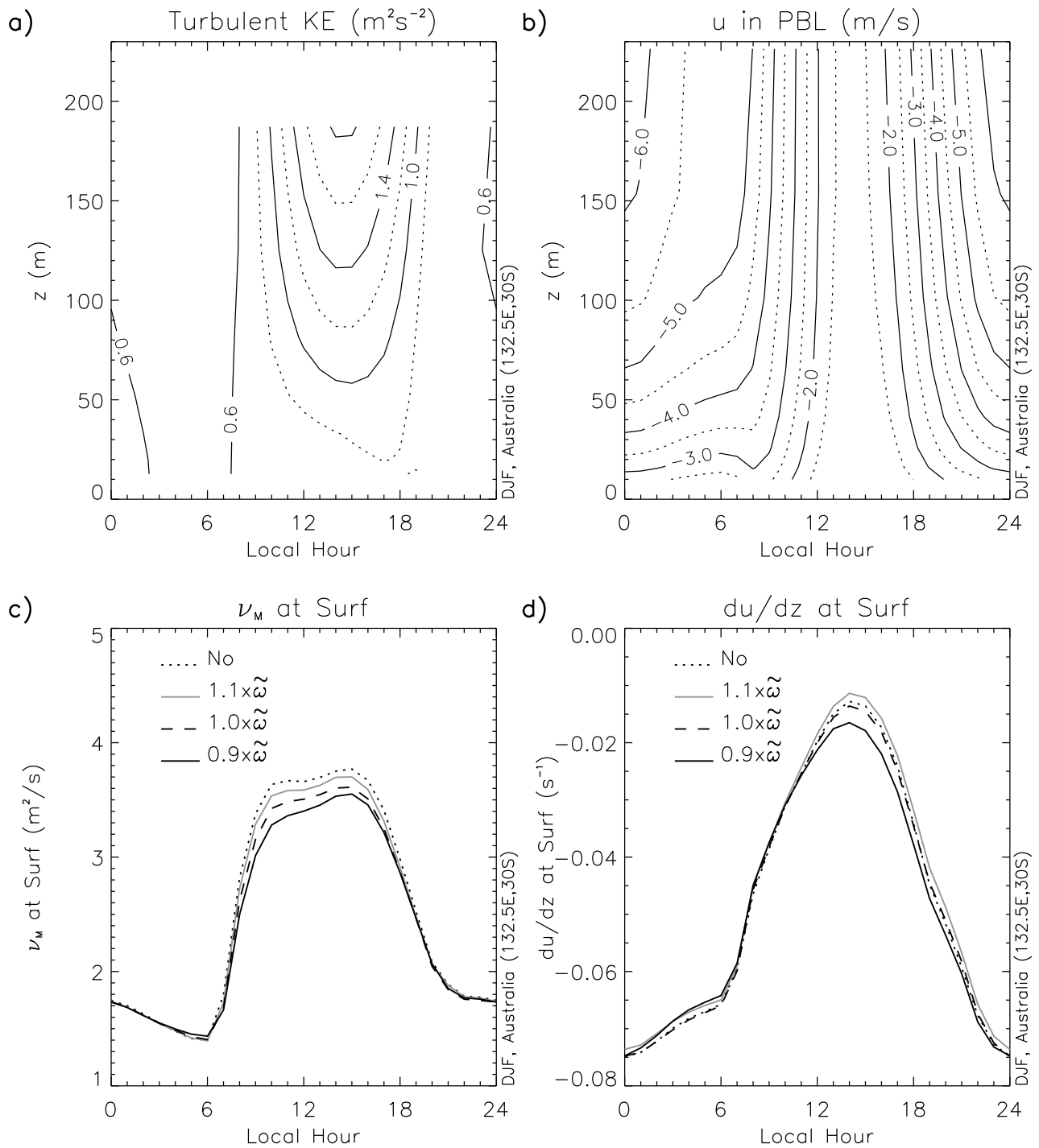


**Figure 7.** DJF diurnal cycle of a) turbulent kinetic energy, b) zonal component of wind within the PBL grid, c) vertical diffusivity of momentum at the surface, and d) shear of the zonal wind on the PBL grid, at the Australian desert source identified in Figure 3b.

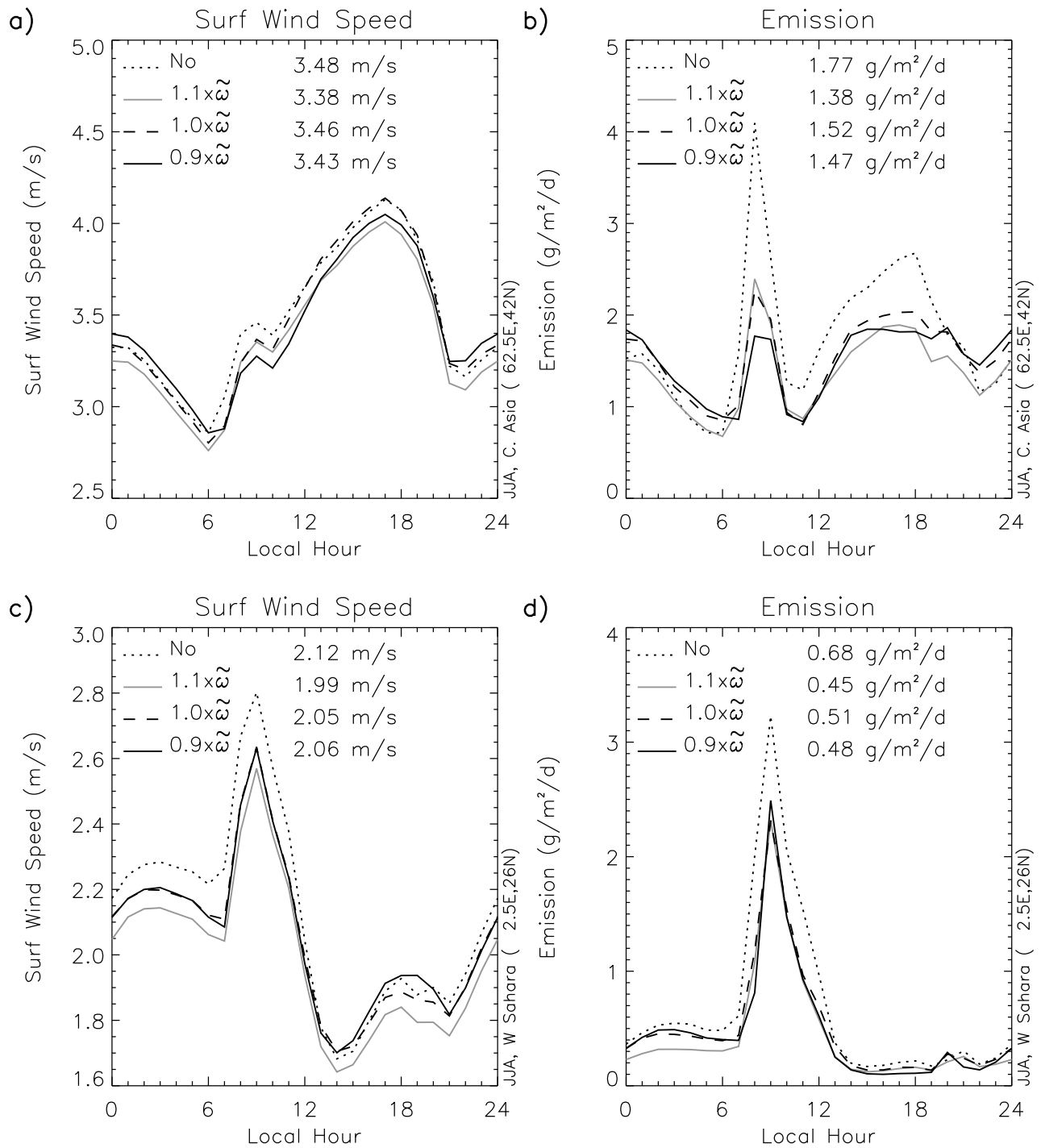


**Figure 8.** JJA diurnal cycle of surface wind speed and dust emission, at the (a,b) Central Asia and (c,d) western Sahara sources identified in Figure 3.

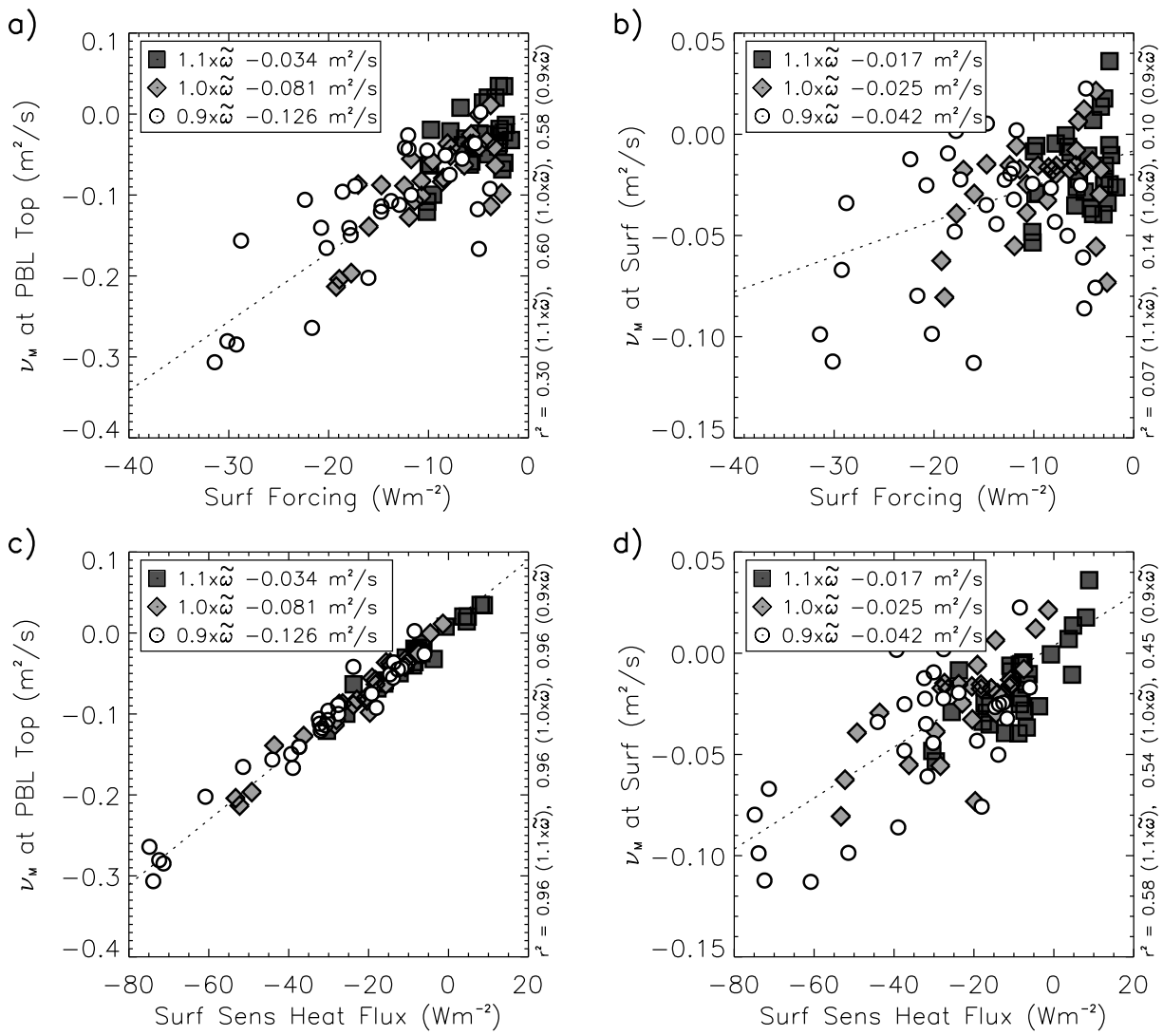


**Figure 9.** Regression of annually averaged anomalies (defined with respect to the experiment omitting dust radiative forcing) as in Figure 5. Regression of surface radiative forcing versus daily maximum value of vertical viscosity at the a) top of the PBL, and b) surface. Regression of the surface sensible heat flux versus daily maximum value of viscosity at the c) top of the PBL, and d) surface. In each panel, the box lists for each experiment the average anomaly for the thirty locations.

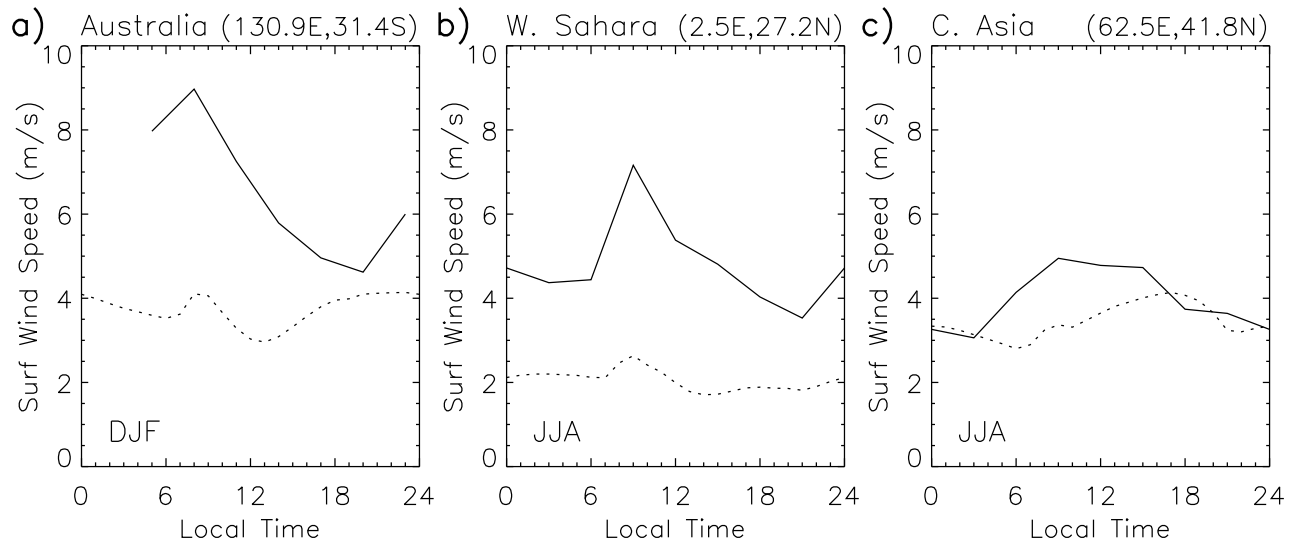


**Figure 10.** Average diurnal cycle of surface wind speed (m/s). The solid line depicts values observed during 1995 at three stations near the AGCM’s most prolific dust sources: a) Nullarbor, Australia (DJF), b) In Salah, Algeria (JJA), and c) Buzaubaj, Uzbekistan (JJA). For comparison, the AGCM values from the baseline experiment with dust radiative forcing ( $1.0 \times \varpi$ ) are replotted from Figs. 6 and 8 as a dotted line.

**Table 1.** Annual average radiative forcing ( $\text{Wm}^{-2}$ ) by dust particles for the globe and the thirty most productive locations for dust emission. The forcing is calculated offline as in *Miller et al.* [2004b] by comparing the radiative fluxes with and without dust. The forcing at the surface and top of the atmosphere (TOA) is listed for particles with baseline optical properties ( $1.0 \times \varpi$ ), along with particles that are more reflecting ( $1.1 \times \varpi$ ) and more absorbing ( $0.9 \times \varpi$ ). Atmospheric heating is the difference of the TOA and surface values. Also shown is the fractional reduction in emission  $\delta\mathcal{E}$ .

	$1.1 \times \varpi$		$1.0 \times \varpi$		$0.9 \times \varpi$	
	Global	Top 30	Global	Top 30	Global	Top 30
<i>Radiative Forcing</i>						
TOA	-0.74	-4.48	-0.17	-0.49	0.82	5.47
Atmos.	-0.22	-1.31	1.38	9.72	3.28	22.04
Surface	-0.96	-5.79	-1.55	-10.21	-2.46	-16.57
<i>Fractional Change in Emission</i>						
$\delta\mathcal{E}$	-0.16	-0.18	-0.17	-0.16	-0.19	-0.16

**Table 2.** Surface radiative forcing ( $\text{Wm}^{-2}$ ) by dust and the wind speed threshold ( $\text{ms}^{-1}$ ) for emission at the four most productive sites for annual emission identified in Figure 2. The forcing represents the JJA average, except for the Australian site, which is for DJF.

Location	Forcing			Threshold
	$1.1 \times \varpi$	$1.0 \times \varpi$	$0.9 \times \varpi$	
W. Sahara	-10.8	-20.4	-29.5	3.3
Australia	-21.8	-33.9	-53.1	4.7
C. Asia	-21.5	-39.1	-65.5	4.6
E. Sahara	-5.9	-12.4	-20.4	4.0

**Table 3.** Correlation  $r$  between the variables regressed with respect to Surface Radiative Forcing and Surface Sensible Heat Flux in Figures 5 and 9. Correlations greater than 0.36 are statistically distinct from zero at the 95% confidence level. The variance accounted for by each regression line is equal to  $r^2$ .

	$1.1 \times \varpi$	$1.0 \times \varpi$	$0.9 \times \varpi$
<i>Surface Radiative Forcing</i>			
Net Rad. at Surf.	0.88	0.95	0.94
Sens. Heat Flux at Surf.	0.67	0.88	0.82
Surf. Wind Speed	0.14	0.37	0.37
Dust Emission	0.30	0.37	0.39
Max. Daily $\nu_M$ at PBL top	0.55	0.78	0.76
Max. Daily $\nu_M$ at PBL base	0.27	0.37	0.32
<i>Sensible Heat Flux at Surface</i>			
Max. Daily $\nu_M$ at PBL top	0.98	0.98	0.98
Max. Daily $\nu_M$ at PBL base	0.76	0.74	0.67